Monthly Notices of the ROYAL ASTRONOMICAL SOCIETY

MNRAS **508,** 1590–1598 (2021) https://doi.org/10.1093/mnras/stab2701
Advance Access publication 2021 September 23

Prospects of direct detection of ^{48}V gamma-rays from thermonuclear supernovae

Fiona H. Panther [1,2,3]★ Ivo R. Seitenzahl [2] Ashley J. Ruiter,[2,3] Thomas Siegert,[4] Stuart Sim[5] and Roland M. Crocker [6]

[1]*Department of Physics, University of Western Australia, Crawley, WA 6009, Australia*
[2]*School of Science, University of New South Wales, Australian Defence Force Academy, Canberra, ACT 2600, Australia*
[3]*Australian Research Council Centre of Excellence for Gravitational Wave Discovery (OzGrav), Australia*
[4]*Center for Astrophysics and Space Sciences, University of California, San Diego, 9500 Gilman Dr., La Jolla, CA 92093-0424, USA*
[5]*Astrophysics Research Centre, School of Mathematics and Physics, Queen's University Belfast, Belfast BT7 1NN, UK*
[6]*The Research School of Astronomy and Astrophysics, Mount Stromlo Observatory, Australian National University, Canberra, ACT 2611, Australia*

Accepted 2021 September 15. Received 2021 September 8; in original form 2021 March 30

ABSTRACT

Detection of gamma-rays emitted by radioactive isotopes synthesized in stellar explosions can give important insights into the processes that power transients such as supernovae, as well as providing a detailed census of the abundance of different isotope species relevant to the chemical evolution of the Universe. Observations of nearby supernovae have yielded observational proof that ^{57}Co powered the late-time evolution of SN1987A's light curve, and conclusive evidence that ^{56}Ni and its daughter nuclei power the light curves of Type Ia supernovae. In this paper, we describe the prospects for detecting nuclear decay lines associated with the decay of ^{48}V, the daughter nucleus of ^{48}Cr, which is expected to be synthesized in large quantities – $M_{\rm Cr} \sim 1.9 \times 10^{-2}\,{\rm M}_{\odot}$ – in transients initiated by explosive helium burning (α-capture) of a thick helium shell. We calculate emergent gamma-ray line fluxes for a simulated explosion model of a thermonuclear explosion of carbon–oxygen white dwarf core of mass $0.45\,{\rm M}_{\odot}$ surrounded by a thick helium layer of mass $0.21\,{\rm M}_{\odot}$. We present observational limits on the presence of ^{48}V in nearby SNe Ia 2014J using the *INTEGRAL* space telescope, excluding a ^{48}Cr production on the surface of more than $0.1\,{\rm M}_{\odot}$. We find that the future gamma-ray mission the All-Sky Medium Energy Gamma-Ray Observatory (AMEGO) will have an approximately 5 per cent chance of observing ^{48}V gamma-rays from such events during the currently planned operational lifetime, based on our birthrate predictions of faint thermonuclear transients. We describe the conditions for a 3σ detection by the gamma-ray telescopes *INTEGRAL*/SPI, Compton Spectrometer and Imager (COSI) , and AMEGO.

Key words: supernovae: general – primordial nucleosynthesis – gamma-rays: general.

1 INTRODUCTION

Detections of gamma-ray line emission at MeV energies allows us to directly observe nucleosynthesis, the process by which the chemical elements are created in stars and stellar end products. Optical spectra – and to some extent photometry – allow us to understand broadly the chemical composition and physical state of material produced by nucleosynthesis, including parameters such as temperature and ionization state. However, optical spectra do not permit the observer to know the isotopic composition of the material they are observing. Observations of gamma-ray spectra can provide direct information about the yield of different isotopes produced by steady-state or explosive nucleosynthesis processes. Understanding the details of nucleosynthesis, and the various abundances of different isotopes that are produced in this process, is critical in enabling us to understand stellar evolution and chemical evolution over cosmic time (see Diehl 2018; Kobayashi, Karakas & Lugaro 2020, for reviews).

Of particular interest is the process of explosive nucleosynthesis that occurs at the end of the lives of stars. Small changes in the properties of the explosion progenitors, the conditions and realization of the explosion can yield significant differences in how explosive nucleosynthesis proceeds and in the final isotopic composition of the explosion ejecta. Such model-dependent differences in the yields of the synthesized radioisotopes have been proposed as discriminants between competing explosion models for Type Ia supernovae (SNe Ia), see e.g. Seitenzahl et al. (2013b, 2015) for the example of radioactive ^{55}Fe or, e.g. Seitenzahl, Taubenberger & Sim (2009) and Röpke et al. (2012) for the ^{57}Ni/^{56}Ni ratio, see also Siebert et al. (2020) and Lach et al. (2020).

Observing the prompt emission gamma-ray lines of radioactive material within the first few hours to hundreds of days post-explosion enables one to understand both the conditions of the explosion and the mechanism that powers other observables such as optical light curves. For example, in 'normal' SNe Ia (Branch & Tammann 1992), the decay of radioisotope ^{56}Ni to ^{56}Co powers the light curve for the first 10 d after maximum light. From 10 d post-maximum, the optical light curve is powered by the decay of ^{56}Co to ^{56}Fe.

★ E-mail: fiona.panther@uwa.edu.au

This mechanism was first proposed as the ultimate source of power radiated in the light curves of SNe Ia in the 1962 PhD thesis of Titus Pankey Jr (Pankey 1962), a theory that was subsequently independently discovered and expanded upon in Colgate & McKee (1969).

The properties and evolution of these light curves form the basis for our understanding of dark energy (Phillips 1993).

In 2014, the first direct observational evidence for ^{56}Ni decay as the mechanism that powers SNe Ia was gathered, confirming Pankey and Colgate's theories. Gamma-ray lines from ^{56}Ni and ^{56}Co decay were observed in the nearby Type Ia supernova SN2014J (Churazov et al. 2014; Diehl et al. 2014) by the two main instruments, SPI and ISGRI, aboard the *INTEGRAL* satellite (Winkler et al. 2003). Detection of these gamma-ray lines also allowed for an accurate determination of the ^{56}Ni mass produced in the explosion (Churazov et al. 2014; Diehl et al. 2014; Isern et al. 2016). Previous to this measurement, gamma-ray derived limits on the production of ^{56}Ni had been derived from SN2011fe, another nearby SNe Ia (Isern et al. 2011; Vedrenne et al. 2003a). Even earlier, COMPTEL observations of SN 1991T have led to claims of detection of ^{56}Co gamma-rays at low significance near the detection threshold (Morris et al. 1995; Morris et al. 1997), but these results are contested (Lichti et al. 1994; Leising et al. 1995).

In the nearby core-collapse supernova, SN1987A, at late times ($>$ 800 days) the light curve stayed bright longer than predicted under the assumption that the light curve was powered by the ^{56}Ni decay chain alone (Kurfess et al. 1992). Subsequent observations discovered gamma-ray lines produced in the decay of ^{57}Co – the first detection of gamma-rays associated with nucleosynthesis beyond the Galaxy (Kurfess et al. 1992). The mass of ^{57}Co determined was sufficient to power the late time light curve (Clayton et al. 1992), and initial tension (Suntzeff et al. 1991, 1992) between the ^{57}Co masses inferred from the direct detection results and the light-curve analysis were reconciled when the effects of freeze-out (Fransson & Kozma 1993; Fransson & Jerkstrand 2015) and internal conversion electrons (Seitenzahl et al. 2009; Seitenzahl, Timmes & Magkotsios 2014) are taken into account.

While normal SNe Ia were initially thought to be powered exclusively by the ^{56}Ni chain, deep observations of nearby SNe Ia (SN 2003hv, SN 2011fe, SN 2012cg, SN 2013aa, SN2014J, ASASSN-14lp, SN2015F) revealed similar slow-downs of their light curves at late-times (Leloudas et al. 2009; Graur et al. 2016, 2018a,b; Kerzendorf et al. 2017; Dimitriadis et al. 2017; Shappee et al. 2017; Yang et al. 2018; Jacobson-Galán et al. 2018; Li et al. 2019), generally attributed to the dominant contribution of ^{57}Co decay to the heating at late times.

Such observations represent just the beginning of our ability to directly interrogate the process of nucleosynthesis in supernovae and other cosmic explosions. Another isotope of particular interest is associated with the synthesis and decay of ^{48}Cr. The isotope ^{48}Cr is synthesized during explosive α-capture, and the short half-life of this radionuclide and its daughter ^{48}V has been proposed as the source that powers the rapidly declining light curves of SN2005E-like supernovae (Waldman et al. 2011), a subclass of SNe first described by Perets et al. (2010) and subsequently studied in more detail by Kasliwal et al. (2012), Yuan et al. (2013), and Lyman et al. (2013). The synthesis of ^{48}Cr in helium detonations and deflagrations has also been investigated by Woosley & Kasen (2011), who demonstrated that significant yields of ^{48}Cr is expected in a variety of models – particularly helium deflagrations – while models that resemble more typical SNe Ia produce substantially less ^{48}Cr. Thus, production of large quantities of ^{48}Cr in thermonuclear supernovae is a characteristic of the presence of a thick helium layer in the progenitor.

The presence of ^{48}Cr and ^{48}V as the dominant isotopes that power the optical light curve of supernovae results in spectroscopic and photometric peculiarities – notably that they are sub-luminous and fast declining compared to 'normal' SNe Ia. This has been noted in several works in which theoretical models of supernovae that produce significant quantities of these radioisotopes were investigated, including Woosley & Kasen (2011), Waldman et al. (2011), and Sim et al. (2012) The rapidly declining light curves of these models are particularly distinctive, following the radioactive decay of the short-lived ^{48}Cr decay chain. It has been proposed, furthermore, that there may be features associated with these isotopes present in the optical spectra of these events (Woosley & Kasen 2011). However, it unfortunately appears that potential spectroscopic features that arise from these atoms are difficult to discriminate from those due to species with similar atomic numbers, namely Ca II and Ti II, at $\sim$ 4000 Å. This serves as an extra motivation to consider, as we do here, the idea that gamma-rays may provide definitive evidence of the presence of ^{48}Cr and ^{48}V as the dominant source of radioactive heating in the ejecta of transients whose progenitors have thick He shells.

^{48}V is of particular interest to observers of gamma-ray lines as it is not only indicative of explosive α-capture in the progenitor explosion, but has an intermediate half-life of $T_{1/2}(^{48}\mathrm{V}) = 15.97$ d that makes it a compelling observational target. At present, the only telescope capable of observing gamma-ray lines such as those produced by the ^{56}Ni decay chain, ^{57}Co and ^{48}V is *INTEGRAL*/SPI. *INTEGRAL*/SPI (Vedrenne et al. 2003b) is ideally suited to observing nuclear decay lines due to its high spectral resolution ($\sim$ 2.7 keV at $\sim$ 20 keV – 8 MeV energies). However, observations of supernovae in even nearby galaxies are limited by the sensitivity of the SPI instrument. The Compton Spectrometer and Imager (COSI; Tomsick et al. 2019), a Compton telescope, is currently under development. COSI will boost the sensitivity to gamma-ray lines at $\sim$ MeV over SPI because of improved background rejection. The capabilities of compact Compton telescopes, such as COSI have been demonstrated through imaging and spectroscopic measurements of the Galactic 511 keV positron–electron annihilation line during a balloon flight of the instrument in 2016 (Kierans et al. 2016, 2020; Siegert et al. 2020). Other future gamma-ray observatories have also been proposed. One such observatory is AMEGO, the All-Sky Medium Energy Observatory (McEnery et al. 2019), a Compton telescope proposed for launch in the early 2030s. AMEGO will combine high sensitivity between 200 keV and 10 MeV (3σ line sensitivity at 1 MeV of 4×10^{-6} ph s^{-1} cm^{-2}, an $\sim$2 order of magnitude improvement on *INTEGRAL*/SPI) with a wide field of view with a spectral resolution of $\sim$ 1 per cent at 1 MeV.

In this paper, we discuss the prospects for detecting prompt gamma-ray emission associated with nucleosynthesis of radioactive ^{48}V in subluminous thermonuclear events based on the hydrodynamic and nucleosynthesis modelling of such explosions in Sim et al. (2012). We discuss the rates and implications of such an event for current and future telescopes capable of detecting MeV gamma-ray line emission, including *INTEGRAL*/SPI, COSI, and AMEGO.

2 THEORY

2.1 Nucleosynthesis

Explosive nuclear burning in detonations in helium layers on top of WDs is typically incomplete, in the sense that rapid expansion of the hot ashes leads to a freeze-out of the nuclear fusion reactions before

Table 1. Select decay radiation of ^{48}V. Source: Burrows (2006).

Energy (keV)	Intensity (per cent)	Radiation type
4.0	35.1	e^- (Auger K)
4.505	2.9	X-ray (Ka2)
4.511	5.8	X-ray (Ka1)
290.3(11)	49.9(4)	e^+
511.0	99.8 (8)	γ (annihil.)
983.525(4)	99.98(4)	γ
1312.106(8)	98.2(3)	γ

nuclear statistical equilibrium is achieved (e.g. Townsley, Moore & Bildsten 2012; Moore, Townsley & Bildsten 2013). Consequently, compared to explosive carbon–oxygen (CO) burning (e.g. Livne & Arnett 1995; Seitenzahl et al. 2013a), the ashes of helium-detonations are overabundant in α-isotopes such as ^{36}Ar, ^{40}Ca, ^{44}Ti, ^{48}Cr, or ^{52}Fe (e.g. Woosley & Weaver 1994; Seitenzahl & Townsley 2017). The most abundant of these α-isotopes is determined by the conditions of the explosion, notably the pre-explosion density (which in turn determines the peak temperature), with successive α-captures proceeding to the heaviest nucleus that can be formed on hydrodynamic time-scales – in this case, ^{48}Cr. Pollution of the helium layer by admixture of, e.g. carbon or oxygen can also result in an 'α-limited burn' and great enhancement of 'stagnation nuclei', with a ratio of ^{4}He to ^{12}C around 4:1 by mass resulting in the greatest production of ^{48}Cr (see section 4.3 of Gronow et al. 2020). These scenarios are unique to helium detonations. Another mode by which these α-isotopes can be synthesized is the so-called α-rich freeze out, which occurs during the carbon detonation or deflagration processes. However, typical masses of α-isotopes produced in this process are much lower, with final yields of $\sim 10^{-6}$ M$_\odot$ of ^{48}Cr in deflagration (e.g. Fink et al. 2014) and $\sim 10^{-4}$ M$_\odot$ of ^{48}Cr in delayed-detonation (e.g. Seitenzahl et al. 2013a) models, and these explosions are characterized as normal SNe Ia based on their light curves as the dominant nuclear product is ^{56}Ni. The helium detonation with which we concern ourselves here is a rarer event, with both spectroscopic and photometric peculiarities described in Sim et al. (2012), where our model is first presented.

^{48}Cr itself is a poor candidate for direct detection with gamma-ray telescopes since the short half-life of $\sim$24 h means that most decays will occur at very high optical depth. Further, any gamma-ray observation would have to be triggered by an initial optical detection of the supernova. By the time the hypothetical supernova becomes optically bright, 2–3 d post-explosion, the majority of the synthesized ^{48}Cr will already have decayed to ^{48}V.

The decay product ^{48}V is a radioisotope of vanadium (atomic number 23), on the proton-rich side of the valley of stability, with a half-life of 15.9735(25) d (Burrows 2006). With a ground state to ground state Q-value of 4012.3(24) keV, the decay to stable ^{48}Ti occurs roughly at 50 per cent via electron capture and 50 per cent via β^+-decay. The decay radiation includes a number of positrons, electrons (both Auger and internal conversion), X-rays, and gamma-rays (both from nuclear transition as well as the 511 keV annihilation line). A very limited selection of the most prominent decay products and their intensities is summarized in Table 2. In this paper, we will focus on the emission of the prominent gamma-rays at 983 and 1312 keV.

The longer half-life of ^{48}V, coupled with its production at relatively low-optical depth in the helium-rich surface layers of sub-luminous thermonuclear supernovae (e.g. Waldman et al. 2011; Sim et al. 2012), means that these two main nuclear gamma-rays are promising direct-detection prospects for future planned missions (see Section 4).

Table 2. Properties of the progenitor system of the studied explosion model. The masses are not independent but are determined from the temperature and density parameters, and the equations of hydrostatic equilibrium. Source: Sim et al. (2012).

Parameter/Unit	Value
CO core central temperature	5×10^7 K
CO core central density	3.81×10^6 g cm^{-3}
He layer base temperature	2×10^8 K
He layer base density	0.592×10^6 g cm^{-3}
CO mass	0.45 M$_\odot$
He layer mass	0.21 M$_\odot$
Total mass	0.66 M$_\odot$
^{48}V mass synthesized	1.9×10^{-2} M$_\odot$

2.2 Description of radiative transfer model

The gamma-ray spectra used to investigate the detectability of ^{48}V are obtained from the output of explosion simulations, nucleosynthesis, and radiation transport simulations described by Sim et al. (2012).

Our general model is based on the explosion simulations studied in Sim et al. (2012). That work explored the outcome of detonations in isolated, low-mass carbon–oxygen white dwarfs (CO WDs) that are surrounded by massive helium shells, regardless of how such a configuration may arise in nature. To assess how such a star may end up with such a configuration – and quantify the birthrates of such systems, which we would expect to only arise in interacting binaries – we use the STARTRACK binary evolution population synthesis code (see below). For this work, we assume that CO WDs may accumulate a non-negligible amount of helium through rapid mass transfer, e.g. during a merger event with a helium-rich star (either a helium or HeCO 'hybrid' white dwarf). We describe our method in Section 4.

We utilize the edge-lit core detonation (ELDD) model of Sim et al. (2012). Specifically, we choose the ELDD-L model as it provides a benchmark for the emission of gamma-rays from the decay of ^{48}V for supernovae that arise from helium detonations. In this model, the detonation of the helium layer ignites the CO core of the progenitor. The parameters of the pre-explosion model can be found in table 1 of Sim et al. (2012) and is replicated here in Table 2 of this paper for clarity.

Details of the explosion simulations, nucleosynthesis, and radiation transport are given by Sim et al. (2012) and Fink et al. (2010). Synthetic observables, including gamma-ray spectra, are derived from the simulations of the ELDD-L model using the ARTIS radiation transport program (Sim 2007; Kromer & Sim 2009). For our analysis, we use the angle-averaged gamma-ray synthetic spectrum for simplicity (note that the underlying explosion models are two-dimensional an therefore predict a degree of dependence on the observer orientation – however, for such variations are modest and not a dominant source of uncertainty for our estimates here). In this model, the dominant radioactive species in the ejecta is ^{48}Cr (and hence its daughter nucleus ^{48}V) that is sythesized by the detonation of the He-layer ($M = 1.9 \times 10^{-2}$ M$_\odot$). Only a small mass of ^{56}Ni is synthesized in the He-layer ($M = 7.6 \times 10^{-3}$ M$_\odot$) and a negligible quantity ($M = 1.5 \times 10^{-7}$ M$_\odot$) in the CO core.

At very early times ($\sim$ hours–day), there is a small contribution to the light curve from ^{52}Fe, however, the bolometric light curve is

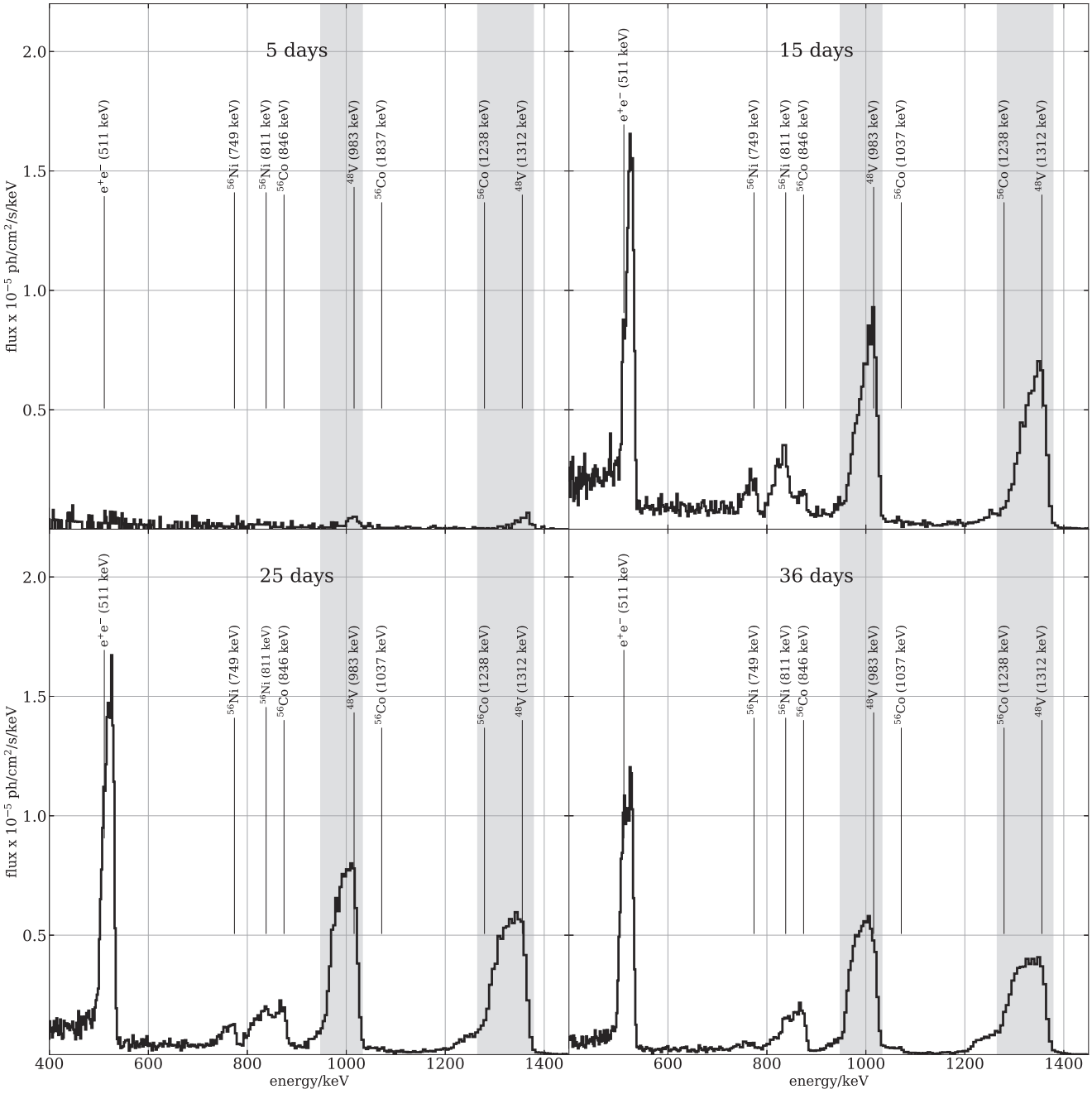

Figure 1. Evolution of the gamma-ray spectrum of ELDD-L model at ∼MeV energies. The gamma-ray spectrum is shown at 5, 15, 25, and 35 d post-explosion. The shaded bands indicate the energies over which the line emission due to the decay of ^{48}V is integrated to compute the light curve for each line. The line centre is approximated to be blueshifted by 10 000 km s^{-1} with respect to the rest frame energy of each ^{48}V gamma-ray line. The minimum of each energy band is then at −20 000 km s^{-1} with respect to the line centre, and the maximum energy is at +5000 km s^{-1} with respect to the line centre. Other characteristic gamma-ray lines are indicated with their rest-frame energies included in brackets. Line emission from positron annihilation (∼ 511 keV) and decay of ^{56}Ni and ^{56}Co are also visible at later times.

mainly powered by the decay of ^{48}Cr and ^{48}V in the early phase, between 3 and 30 d post-explosion.

Almost all radioactive material is located in the He-layer ejecta at low optical depths, and consequently some of the gamma-rays from these decays are able to escape.

The escaping gamma-rays give rise to line emission at ∼ MeV energies (Table 1) that might be detected by space-based telescopes.

3 SIMULATED OBSERVATIONS

We simulate the gamma-ray emission from a supernova that results from the ELDD-L model of Sim et al. (2012) with the event located at a canonical distance of 1 Mpc. The optical properties of this explosion model – spectra and light curve – are presented in detail in Sim et al. (2012). The spectra produced by the model are shown in Fig. 1 at a range of different times post-explosion. The

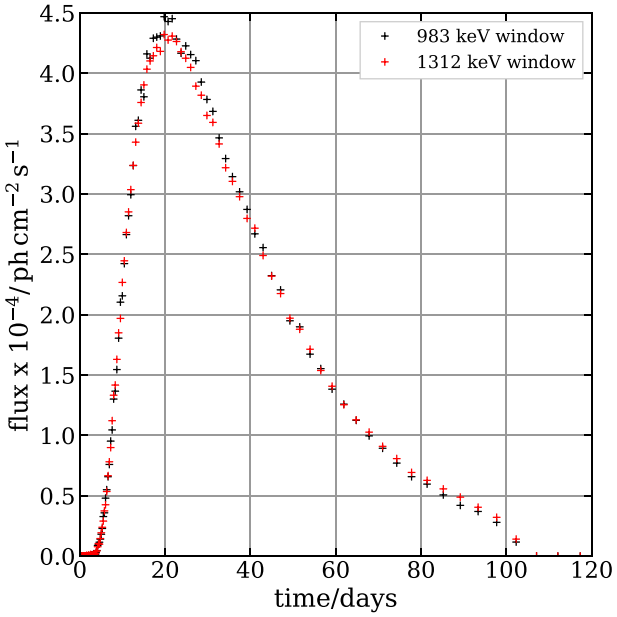

Figure 2. Gamma-ray light curve for ELDD-L model 983 and 1312 keV gamma-ray line emission in the energy bands defined in Fig. 1 for a supernova at a canonical distance of 1 Mpc. At 70 d post-explosion, ^{56}Co emission becomes comparable to the strength of the ^{48}V lines, resulting in the slight plateau visible in the light curve.

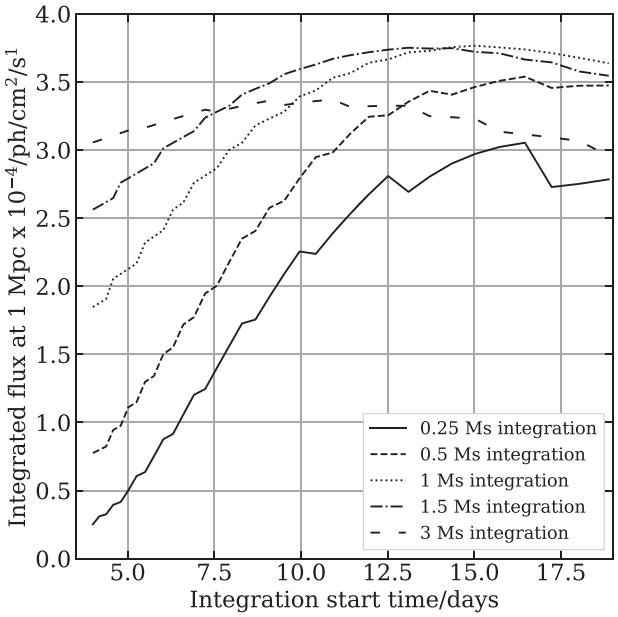

Figure 3. How the time-integrated flux of the ^{48}V 1312 keV line for the ELDD-L model at 1 Mpc varies as a function of the time at which the integration is started. Observations that begin close to maximum light yield the maximum integrated flux for a given observation time. We also find that the optimal integration time is $\sim$ 1–1.5 Ms.

two prominent emission lines result from the decay of ^{48}V. Unlike normal SNe Ia, where ^{56}Co dominates, emission from ^{56}Co is very weak in comparison to the ^{48}V line.

We use these spectra to compute the light curve of each emission line associated with ^{48}V decay. The emission lines are numerically integrated in the window shown by the shaded region in Fig. 1. These regions are defined as follows: The offset of the line centre with respect to the lab energy of each line, which represents the bulk motion of the ejecta, is blueshifted. We determine this blueshift to be well approximated at a velocity of $10,000\,\mathrm{km\,s^{-1}}$. We then define the lower bound of the integration region to be redshifted by $20,000\,\mathrm{km\,s^{-1}}$ with respect to the line centre for each emission line. This redshift is due to a combination of the velocity of the ash and Compton scattering. The upper bound of the integration region is then defined to be blueshifted by $5,000\,\mathrm{km\,s^{-1}}$ with respect to the line centre. Defining the integration region in velocity space ensures both lines, which arise from the same material with the same kinematics, are treated identically. The bounds of the energy bands are found to be $\sim$ 950–1030 keV for the 983 keV window and $\sim$ 1265–1380 keV for the 1312 keV window. We numerically integrate the flux in each of these windows at each time sample from 0 to 120 d via numerical integration, implemented using the PYTHON `numpy` library function `numpy.trapz` where each bin is defined by the original binning of the spectrum. The effect of choosing these broad energy bands on the detection sensitivity is discussed in Section 4.

Using the gamma-ray light curve, we can determine how to achieve an observation that maximizes the observable flux in a given observation time. We consider observation times of 0.25, 0.5, 1, 1.5, and 3 Ms, typical of the time that would awarded to a target of opportunity observation. We calculate the observed flux of the ELDD-L model at the canonical distance of 1 Mpc for each of these windows beginning at a different initial time t_{start} based on the light curve in Fig. 2. In Fig. 3, we demonstrate that for a given integration time, beginning the integration several days before the peak of the light curve (12–14 d) maximizes the integrated flux that can be observed for a given integration time. We also find that the maximum observable flux saturates with an integration time of 1–1.5 Ms. The subsequent calculations for the detectability of ^{48}V are performed for an integration time of 1.5 Ms beginning at 12.5 d post-explosion.

4 PROSPECTS FOR DETECTABILITY

The sensitivity of a gamma-ray instrument is dependent on several factors, including the integration time of the observation, the energy resolution of the instrument, the detector collecting area, and the background. In this work, we will account for the impact of both the integration time of the observation and the energy resolution of the given instrument. We utilize published 3σ sensitivity curves and detector resolution at 1 MeV for the narrow-line sensitivity of *INTEGRAL*/SPI (e.g. Attié et al. 2003; Diehl et al. 2018, see also[1]) and AMEGO (McEnery et al. 2019). The sensitivity of the COSI instrument was communicated via private communication with T. Siegert and the COSI collaboration. For a given 3σ, 1 Ms sensitivity, the 3σ sensitivity $S_{3\sigma}$ for an observation with a given time t_{o} Ms over a line with FWHM of E_{band} keV for an instrument with a narrow line sensitivity of E_{line} keV is given by

$$S_{3\sigma}(t_{\mathrm{o}}) = S_{3\sigma}\sqrt{\frac{1\,\mathrm{Ms}\times E_{\mathrm{band}}}{t_{\mathrm{o}}E_{\mathrm{line}}}}.$$

Because the observed emission line is significantly broader than the resolution of the telescope, there is a reduction in the sensitivity given by $f_{\mathrm{broad}} = \sqrt{\mathrm{FWHM}/E_{\mathrm{line}}}$ included in the determination of the 3σ sensitivity calculation.

[1] https://www.cosmos.esa.int/web/integral/observation-time-estimator

Table 3. Maximum distances (in Mpc) at which an observation of ^{48}V decay from our model can be made, based on existing (for *INTEGRAL*/SPI) and predicted (for COSI and AMEGO) narrow-line sensitivity of the instruments.

Exposure time (Ms)	*INTEGRAL*/SPI d_{max} (Mpc)	COSI d_{max} (Mpc)	AMEGO d_{max} (Mpc)
	At 983 keV		
1	2.11	3.69	6.29
1.5	2.33	4.08	6.96
	At 1312 keV		
1	2.08	3.65	6.22
1.5	2.08	4.03	6.89

We calculate the maximum distance d_{max} at which a 3σ detection of each ^{48}V line with an integrated flux of F ph cm^{-2} s^{-1} at the canonical distance of 1 Mpc can be made for a given exposure time (Table 3), where

$$d_{max}(t_o) = 1\,\mathrm{Mpc} \times \sqrt{\frac{F}{S_{3\sigma}(t_o)}}.$$

To determine the rate of events that would yield a detection of ^{48}V as a function of d_{max}, we calculate the mass currently contained in stars in the local universe. A summary of measurements of the local stellar mass density is given in Karachentsev & Telikova (2018). We utilize the MK11 measurement of Makarov & Karachentsev (2011) shown in fig. 4 of Karachentsev & Telikova (2018) to compute the enclosed mass of stars as a function of distance.

As stated above, the binary population synthesis code `StarTrack` (Belczynski, Kalogera & Bulik 2002; Belczynski et al. 2008; Ruiter et al. 2014) is used to estimate the number of star systems that could give rise to ELDD-L-like explosions. The primary goal of the Sim et al. (2012) study was to examine what a low-mass exploding CO WD may look like, and though CO WD masses were chosen based on population synthesis models, the final 1D hydrostatic configuration was not based on any specific binary evolution calculation. Our goal here, however, is to assess the likelihood of observing gamma-ray emission from exploding white dwarfs of relatively low mass, i.e. CO WDs that are too low density to explode as 'normal' SNe Ia (see e.g. Barstow 2020). In order to achieve a situation where a relatively low-mass CO WD has a massive helium layer on its surface, the CO WD should be accreting from (or has recently accreted from) a star containing a substantial amount of helium on the surface. While certain binary configurations involving stable (Roche lobe overflow on a nuclear or thermal timescale) mass transfer will lead to helium-burning on the WD surface (e.g. converting the helium to carbon, thereby removing helium), there are certain regions of parameter space during stable Roche lobe overflow where helium will be accumulated on the CO WD and will not burn (Piersanti, Tornambé & Yungelson 2014). Is is also plausible that a somewhat low-mass CO white dwarf with a rather thick helium surface layer could be realized through a merging event (Crocker et al. 2017), though detailed studies of such a situation remain largely unexplored, particularly in 3D (but see Pakmor et al. 2021).

Our population of thermonuclear events should consists of both (1) CO WDs of low-enough mass such that they would produce very little radioactive nickel in a detonation and (2) a non-negligible layer of helium on the WD surface to allow for a shell detonation. We find that rapid mass transfer (e.g. a merger) between a CO white dwarf star and a helium-rich degenerate companion is the most likely scenario in terms of absolute numbers, given these two main constraints. This merger configuration, unlike the slow Roche lobe overflow configuration where mass transfer proceeds on non-dynamical timescales, could plausibly lead to the formation of a star with an inner CO core of relatively low mass ($\lesssim 0.55\,M_\odot$) surrounded by a He-rich outer layer. Systems with similar properties were already discussed in Crocker et al. (2017) as plausible candidates for low luminosity thermonuclear supernovae.

Binary star systems leading to the formation of a CO WD that accretes helium-rich matter via slow Roche lobe overflow from a white dwarf containing helium on its surface have been discussed in (Ruiter et al. 2011, 2014). While in those works it was assumed that mass transfer would be stable in most cases when the stellar mass ratio was above a certain threshold, e.g. when the primary WD is notably more massive than the secondary (Belczynski et al. 2008), it is possible that in such systems, mass transfer becomes unstable, and the two stars actually merge (e.g. see Shen 2015). However, the stable Roche lobe overflow in the population synthesis studies discussed above found that the WD mass was typically larger than required for our study (cf. fig. 2 Ruiter et al. 2014), thus we do not include these types of systems in our rate estimate. In our estimate of birthrates of thermonuclear transients involving helium shell detonations, we consider mergers between CO WDs and WDs that are either 'fully' helium-rich or contain helium-rich mantles on top of a CO core; HeCO 'hybrid' WDs (Iben & Tutukov 1985). It turns out that most merging systems consist of a CO WD (we set the upper mass limit to 0.55 $M_\odot$ as discussed above) and a hybrid WD. Such WDs are formed only in binary systems when a red giant branch star experiences substantial mass-loss, in this case during a common envelope event. The most prominent formation channel leading to our desired binary configuration consists of a stable phase of Roche lobe overflow (from the primary star in the Hertzsprung Gap and/or on the red giant branch donating mass to the MS secondary) → a phase of unstable mass transfer (the now red giant secondary loses its envelope, while the primary is a CO WD; the CE leaves behind a hydrogen-stripped, helium-burning star) → a final phase of stable Roche lobe overflow but this time, the stripped He-burning star donates mass to the CO WD. At some stage the secondary evolves into a hybrid WD, and eventually the larger star (the hybrid) fills its Roche lobe. This time mass transfer is unstable, and the stars are presumed to merge. To translate our simulated events into predicted events, we calibrate our raw model data (∼3000 systems) by tracking the mass born in stars for our simulation and scale this to the estimated mass in stars in the observed sample volume assuming a binary fraction of 70 per cent. We emphasize that our rate estimate should be taken as a lower limit, since we are not including the (more numerous) systems that are presumed to encounter stable Roche lobe overflow in the code.

In Fig. 4, we show the rate of such systems per ten years (an optimistic extended lifetime for space-based observatories) as a function of d_{max}. These rates are a lower limit as we calculate rates based on the present-day mass in stars. For the most optimal

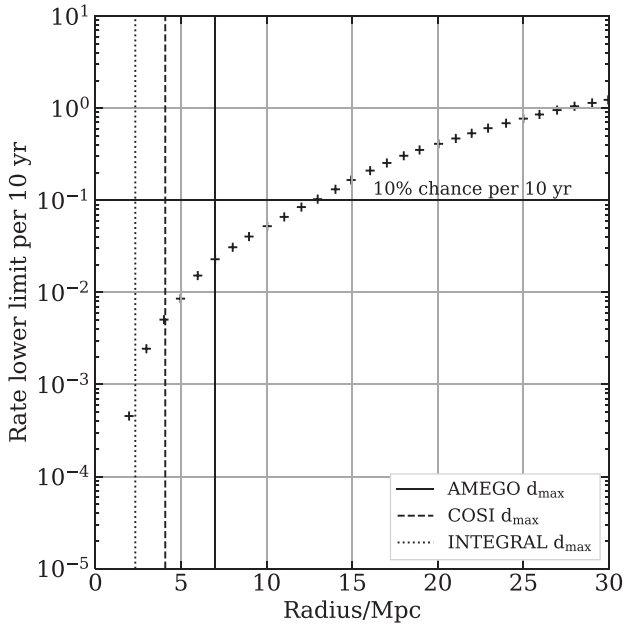

Figure 4. Rate per 10 yr of ^{48}V-line emitting supernovae determined from binary population synthesis calculations and the stellar density in the local volume. Over a 10 yr mission we estimate a $\sim$ 5 per cent chance of observing such an event. While the probability of such an event is low, a nearby SNe Ia would provide interesting constraints on nucleosynthesis of ^{48}V.

observation (1.5 Ms with AMEGO) we find a lower limit to the event rate to be 0.02 per 10 yr (i.e. a 2 percent chance of a successful observation within a 10 yr mission lifetime.

5 OBSERVATIONAL LIMITS FROM PREVIOUS OBSERVATIONS OF SN2014J

During the lifetime of *INTEGRAL*, only two thermonuclear supernovae were close enough to be within reach for meaningful measurements: SN2011fe in M101 (Nugent et al. 2011) and SN2014J in M82 (Fossey et al. 2014). While SN2011fe has not been detected in gamma-rays (Isern et al. 2011), SN2014J merited an observation campaign for about half a year and led to the first detection of gamma-rays from ^{56}Co from the core of an exploding WD (Churazov et al. 2014; Diehl et al. 2015). Early observations, only 16 d after the explosion date, also found gamma-rays from the decay of the shorter lived parent-nucleus ^{56}Ni, which was interpreted as the production of $\sim 0.06\,M_\odot$ of ^{56}Ni on the surface of the WD (Diehl et al. 2014; Isern et al. 2016). These early observations are also close to the optimal point for the search of ^{48}V (see Fig. 3), so that we can compare our model expectations with this observation.

Between 16.3 and 30 d (i.e. $\sim$ 1.2 Ms), the 983 and 1312 keV lines are not detected. Assuming a line broadening of 10000 km s^{-1}, the 3σ flux limits during this period are 2.4×10^{-4} and 2.1×10^{-4} ph cm^{-2} s^{-1} for the 983 and 1312 keV line, respectively. Given the distance to SN2014J of 3.3 Mpc (Foley et al. 2014), these limits are about 5–6 times larger than what would be expected in our model. This excludes a ^{48}Cr production on the surface of more than $0.1\,M_\odot$. While these values are hardly constraining, it is important to show the consistency between the expectations of this high-^{48}Cr-yield model and observations, especially because SN2014J also showed significant contributions of nucleosynthesis products on its surface. Later observations, for example, between 50 and 70 d after the explosion, are less constraining, even though the flux limits drop to 1.6×10^{-4} and 1.3×10^{-4} ph cm^{-2} s^{-1} for the 983 and 1312 keV line, respectively.

We note that while *INTEGRAL* is unable to provide measurements of emission from ^{48}V decay in SN2014J (and hence constraints on the model of Diehl et al. (2015) that proposes the presence of helium-rich material in the explosion), had AMEGO or COSI been operational when the event occurred then this model could have been either confirmed or falsified, based on the above constraints from *INTEGRAL*.

6 DISCUSSION

The scope of this work is to investigate the feasibility of an observation of radioisotope decay that is characteristic of the thermonuclear explosion of massive helium shells. While the presence of ^{48}Cr and its daughter nuclei have significant implications for the optical light curves and spectra of these supernovae (Waldman et al. 2011; Woosley & Kasen 2011; Sim et al. 2012), definitive evidence for their presence as the dominant product of helium detonation (or deflagration) can be obtained through gamma-ray line observations. We note some potential avenues for detector improvement to enable such a detection, and the limitations of our rate estimations used in this work.

Increasing the sensitivity of detectors can have a significant impact on the probability of detecting gamma-ray emission from supernovae. For example, a factor of 2 improvement in the sensitivity of AMEGO at 1 MeV increases d_{max} to $\sim$ 9 Mpc. This would double the rate of observable events per ten years (see Fig. 4).

In this paper, we consider gamma-ray observatories that can make both wide field-of-view observations of diffuse emission and observations of point sources such as supernovae. A factor of $\sim$6 improvement of the sensitivity of an instrument to observe large areas at once, such as AMEGO or COSI, and improved background suppression and rejection could enable serendipitous detection of gamma-rays from supernovae as far out as the Virgo cluster, at a distance of $\sim$16.5 Mpc.

AMEGO and COSI are optimized to observe large areas of the sky. Telescopes that are optimized to observe point sources of MeV gamma-rays are more ideally suited to carry out the observations described in this paper. For example, the proposed Lunar Occultation Observatory (LOX; Miller & Lawrence 2016) uses lunar occultation as a method of observing gamma-rays from point sources. Lunar occultation enables detector background, which limits detector sensitivity, to be removed with much greater efficacy. Coupled with the intrinsically lower background due to the proposed observatory's lunar orbit, LOX's sensitivity could enable the detection of ^{56}Ni and ^{56}Co in SNe Ia out to $\sim$ 10 Mpc. Comparing the flux of the ^{56}Ni and ^{56}Co lines found in SN2014J in Diehl et al. (2014) to that of the ^{48}V emission in our analysis, we find that an observatory like LOX can detect ^{48}V emission at comparable distances.

Alternative MeV gamma-ray telescopes optimized for observing point sources include Laue lenses, which use the principle of Laue diffraction of gamma-rays in a lens made of high-purity Ge crystals to focus gamma-rays into the detector plane. Laue lenses have been proposed for astronomy applications, particularly observing $\sim$MeV emission from point sources, however most designs for such a telescope are currently highly experimental.

The scope of this paper is to focus on the feasibility of detecting observational signatures that are unique to thermonuclear detonation of massive helium shells. Consequently, the rate estimated in this

work is primarily theoretical and based on binary evolution calculations, although motivated by trying to understand the processes that may occur in thermonuclear supernovae that are not powered primarily by nickel and cobalt decay. Consequently, our calculated rate for ELDD-L-like events has some uncertainties.

In our calculation of the expected event rate as a function of distance, we consider only the mass that is presently contained in stars. This results in an underestimate of supernova rates from systems with long-delay times (e.g. Panther et al. 2019), as it does not take into account the total mass that formed into stars – most massive stars that formed in the past will have since exploded as supernovae. As the binary population synthesis calculation depends on knowing the total mass that formed into stars, our calculation underestimates the rate. However, since most of the stellar mass is contained in low-mass stars, the approximation we use for this work is reasonable to obtain a lower limit.

The model used in this work is comprised of a low-mass CO WD core surrounded by a thick helium envelope. Our rate is calculated based on the incidence of interacting binary systems that may end their lives in such configurations. We consider all systems that involve mergers of low mass CO WDs and helium hybrid WDs, and consequently the rate we estimate is somewhat uncertain and may be a factor of a few larger or smaller, depending on the kind of evolutionary tracks that could give rise to these mergers. However, we point out that any thermonuclear explosion of a system with a massive helium shell is expected to synthesize considerable quantities of ^{48}Cr, and consequently is expected to emit gamma-rays from the decay of daughter nucleus ^{48}Cr (e.g. see the model of SN2014J proposed by Diehl et al. 2015). This is a unique feature of massive helium shell detonations. Some simulations involving higher mass CO WD cores have been carried out (e.g. Pakmor et al. 2021), which yield interesting synthetic observables that may be of interest in the era of large-scale surveys by the likes of the Vera C. Rubin Observatory.

During the accretion process, nuclear burning on the CO WD core may result in the emission of X-rays giving rise to so-called supersoft X-ray sources (Woods & Gilfanov 2016). These sources are not readily detectable beyond the Large Magellanic Cloud, making a detectable event very unlikely with existing or future technology. For low-mass CO WDs, such as in our scenario, radiation emitted during the accretion process would be predominantly emitted in the far-UV, which is mostly attenuated by interstellar dust and gas in the host galaxy.

Further work is required to understand the explosion properties of configurations involving low mass CO WD cores with thick helium envelopes, especially in the case of low mass CO WD cores. Such systems are of general interest and have been proposed to be a significant source of Galactic antimatter (Crocker et al. 2017).

7 CONCLUSIONS

In this paper, we discuss the prospects for observing gamma-ray line emission from supernovae predominantly powered by the decay of the intermediate mass element ^{48}Cr and its daughter nuclei. We outline an optimized observing strategy based on radiative transfer models of edge-lit double detonation of a CO WD with a He layer. We compute gamma-ray light curves for the two dominant emission lines of ^{48}V and determine that an optimal, idealized observation strategy would involve a $1 - 1.5$ Ms exposure beginning at ~ 12 d post-explosion. We determine the maximum distances at which a SN explosion exhibiting the V lines similar to that of the model could be observed with 3σ significance, taking into account the broad linewidth reducing the sensitivity of each instrument. Finally, we estimate a rate for such events based on binary population synthesis calculations.

While we find the rates of such events to be relatively low, we note that the highly random nature of SN events in the local Universe may mean that we could see a nearby event – such as SN2014J, SN2011fe, or even as close as SN1987A – by virtue of chance. Moreover, we note that the link between the explosion model and the progenitor system rate determined from our binary evolution calculation introduces additional uncertainty. Observation of ^{48}V emission, a radioisotope only synthesized in significant quantities by thermonuclear detonation of massive helium shells is highly model discriminating. Based on our calculations and the success of observations of gamma-ray lines from other nearby thermonuclear supernovae, we conclude that the potential to directly observe the radioactive decay of Cr and V produced in detonations of massive helium shells on top of white dwarf stars is a real possibility with proposed future gamma-ray instruments.

ACKNOWLEDGEMENTS

The authors wish to thank the reviewer for their constructive comments to improve the paper. This research was conducted in Canberra, on land for which the Ngunnawal and Ngambri people are the traditional and ongoing custodians, and in Perth, on land for which the Wadjuk Noongar people are the traditional and ongoing custodians. Analysis of synthetic spectra was performed using the open-source PYTHON library NUMPY (van der Walt, Colbert & Varoquaux 2011), and all plots are generated using the open-source MATPLOTLIB PYTHON library (Hunter 2007). FHP is supported by the Australian Research Council (ARC) Centre of Excellence for Gravitational Wave Discovery (OzGrav) under grant CE170100004. TS is supported by the German Research Society (DFG-Forschungsstipendium SI 2502/1-1 and 2502/3-1). IRS and AJR are supported by the Australian Research Council through grant numbers FT160100028 and FT170100243, respectively. RMC acknowledges funding from Australian Research Council award DP190101258 shared with Prof. Mark Krumholz at the ANU. SAS acknowledges travel support from the Australian National University's, Research School of Astronomy & Astrophysics, Distinguished Visitor Program and the ARC Centre for Excellence for All-sky Astrophysics (CAASTRO) for travel to Australia in 2017, which contributed to part of this work. This research was undertaken with the assistance of resources and services from the National Computational Infrastructure (NCI), which is supported by the Australian Government, through the National Computational Merit Allocation Scheme and the UNSW HPC Resource Allocation Scheme. We thank Roland Diehl and Sandra Resch for providing limits on Vanadium lines in SN2014J.

DATA AVAILABILITY

The data and programs used to analyse the data are available via GitHub at https://github.com/fipanther/Vlineprospects. The repository enables the results presented in this work to be replicated and the spectrum of this model (including optical emission) to be explored if the reader desires. For more information on the models themselves, we direct the reader to the orignal work of Sim et al. (2012) where the model and its optical characteristics were presented. Any use of the provided models must cite the original work of Sim et al. (2012).

REFERENCES

Attié D. et al., 2003, A&A, 411, L71
Belczynski K., Kalogera V., Bulik T., 2002, ApJ, 572, 407
Belczynski K., Kalogera V., Rasio F. A., Taam R. E., Zezas A., Bulik T., Maccarone T. J., Ivanova N., 2008, ApJS, 174, 223
Branch D., Tammann G. A., 1992, ARA&A, 30, 359
Burrows T., 2006, Nucl. Data Sheets, 107, 1747
Churazov E. et al., 2014, Nature, 512, 406
Clayton D. D., Leising M. D., The L.-S., Johnson W. N., Kurfess J. D., 1992, ApJ, 399, L141
Colgate S. A., McKee C., 1969, ApJ, 157, 623
Crocker R. M. et al., 2017, Nat. Astron., 1, 0135
Diehl R., 2018, Astrophysics with Radioactive Isoptopes. Springer, Berlin, p. 3
Diehl R. et al., 2014, Science, 345, 1162
Diehl R. et al., 2015, A&A, 574, A72
Diehl R. et al., 2018, A&A, 611, A12
Dimitriadis G. et al., 2017, MNRAS, 468, 3798
Fink M., Röpke F. K., Hillebrandt W., Seitenzahl I. R., Sim S. A., Kromer M., 2010, A&A, 514, A53
Fink M. et al., 2014, MNRAS, 438, 1762
Foley R. J. et al., 2014, MNRAS, 443, 2887
Fossey S. J., Cooke B., Pollack G., Wilde M., Wright T., 2014, Cent. Bur. Electron. Telegrams, 3792, 1
Fransson C., Jerkstrand A., 2015, ApJ, 814, L2
Fransson C., Kozma C., 1993, ApJ, 408, L25
Graur O., Zurek D., Shara M. M., Riess A. G., Seitenzahl I. R., Rest A., 2016, ApJ, 819, 31
Graur O. et al., 2018a, ApJ, 859, 79
Graur O., Zurek D. R., Cara M., Rest A., Seitenzahl I. R., Shappee B. J., Shara M. M., Riess A. G., 2018b, ApJ, 866, 10
Gronow S., Collins C., Ohlmann S. T., Pakmor R., Kromer M., Seitenzahl I. R., Sim S. A., Röpke F. K., 2020, A&A, 635, A169
Hunter J. D., 2007, Comput. Sci. Eng., 9, 90
Iben I. J., Tutukov A. V., 1985, ApJS, 58, 661
Isern J. et al., 2011, Astron. Telegram, 3822, 1
Isern J. et al., 2016, A&A, 588, A67
Jacobson-Galán W. V., Dimitriadis G., Foley R. J., Kilpatrick C. D., 2018, ApJ, 857, 88
Karachentsev I. D., Telikova K. N., 2018, Astron. Nachr., 339, 615
Kasliwal M. M. et al., 2012, ApJ, 755, 161
Barstow M. A. et al., 2020, in Barstow M. A.et al., Proc. of the IAU, Vol. 357, White Dwarfs as Probes of Fundamental Physics: Tracers of Planetary, Stellar and Galactic Evolution. Cambridge Univ. Press, Cambridge
Kerzendorf W. E. et al., 2017, MNRAS, 472, 2534
Kierans C. et al., 2016, Proceedings in 11th INTEGRAL Conference: Gamma-Ray Astrophysics in Multi-Wavelength Perspective, The 2016 Super Pressure Balloon flight of the Compton Spectrometer and Imager. Amsterdam, The Netherlands
Kierans C. A. et al., 2020, ApJ, 895, 44
Kobayashi C., Karakas A. I., Lugaro M., 2020, ApJ, 900, 179
Kromer M., Sim S. A., 2009, MNRAS, 398, 1809
Kurfess J. D. et al., 1992, ApJ, 399, L137
Lach F., Röpke F. K., Seitenzahl I. R., Coté B., Gronow S., Ruiter A. J., 2020, A&A, 644, A118
Leising M. D. et al., 1995, ApJ, 450, 805
Leloudas G. et al., 2009, A&A, 505, 265
Li W. et al., 2019, ApJ, 882, 30
Lichti G. G. et al., 1994, A&A, 292, 569
Livne E., Arnett D., 1995, ApJ, 452, 62
Lyman J. D., James P. A., Perets H. B., Anderson J. P., Gal-Yam A., Mazzali P., Percival S. M., 2013, MNRAS, 434, 527
Makarov D., Karachentsev I., 2011, MNRAS, 412, 2498
McEnery J. et al., 2019, in Bull. Am. Astron. Soc., 51, 245
Miller R. S., Lawrence D. J., 2016, ApJ, 823, L31
Moore K., Townsley D. M., Bildsten L., 2013, ApJ, 776, 97
Morris D., Bennett K., Bloemen H., Hermsen W., Lichti G., McConnell M. L., Ryan J., Schoönfelder V., 1995, Ann. New York Acad. Sci., 759, 397
Morris D. J. et al., 1997, AIPC, 410, 1084
Nugent P., Sullivan M., Bersier D., Howell D. A., Thomas R., James P., 2011, Astron. Telegram, 3581, 1
Pakmor R., Zenati Y., Perets H. B., Toonen S., 2021, MNRAS
Pankey Titus J., 1962, PhD thesis, Howard University
Panther F. H., Seitenzahl I. R., Ruiter A. J., Crocker R. M., Lidman C., Wang E. X., Tucker B. E., Groves B., 2019, Publ. Astron. Soc. Aust., 36, e031
Perets H. B. et al., 2010, Nature, 465, 322
Phillips M. M., 1993, ApJ, 413, L105
Piersanti L., Tornambé A., Yungelson L. R., 2014, MNRAS, 445, 3239
Röpke F. K. et al., 2012, ApJ, 750, L19
Ruiter A. J., Belczynski K., Sim S. A., Hillebrand t W., Fryer C. L., Fink M., Kromer M., 2011, MNRAS, 417, 408
Ruiter A. J., Belczynski K., Sim S. A., Seitenzahl I. R., Kwiatkowski D., 2014, MNRAS, 440, L101
Seitenzahl I. R., Townsley D. M., 2017, Nucleosynthesis in Thermonuclear Supernovae. Springer International Publishing, Cham, p. 1955
Seitenzahl I. R., Taubenberger S., Sim S. A., 2009, MNRAS, 400, 531
Seitenzahl I. R. et al., 2013a, MNRAS, 429, 1156
Seitenzahl I. R., Cescutti G., Röpke F. K., Ruiter A. J., Pakmor R., 2013b, A&A, 559, L5
Seitenzahl I. R., Timmes F. X., Magkotsios G., 2014, ApJ, 792, 10
Seitenzahl I. R. et al., 2015, MNRAS, 447, 1484
Shappee B. J., Stanek K. Z., Kochanek C. S., Garnavich P. M., 2017, ApJ, 841, 48
Shen K. J., 2015, ApJ, 805, L6
Siebert M. R., Dimitriadis G., Polin A., Foley R. J., 2020, ApJ, 900, L27
Siegert T. et al., 2020, ApJ, 897, 45
Sim S. A., 2007, MNRAS, 375, 154
Sim S. A., Fink M., Kromer M., Röpke F. K., Ruiter A. J., Hillebrandt W., 2012, MNRAS, 420, 3003
Suntzeff N. B., Phillips M. M., Depoy D. L., Elias J. H., Walker A. R., 1991, AJ, 102, 1118
Suntzeff N. B., Phillips M. M., Elias J. H., Depoy D. L., Walker A. R., 1992, ApJ, 384, L33
Tomsick J. et al., 2019, in Bull. Am. Astron. Soc., 51, 98
Townsley D. M., Moore K., Bildsten L., 2012, ApJ, 755, 4
van der Walt S., Colbert S., Varoquaux G., 2011, Comput. Sci. Eng., 13, 22
Vedrenne G. et al., 2003a, A&A, 411, L63
Vedrenne G. et al., 2003b, A&A, 411, L63
Waldman R., Sauer D., Livne E., Perets H., Glasner A., Mazzali P., Truran J. W., Gal-Yam A., 2011, ApJ, 738, 21
Winkler C. et al., 2003, A&A, 411, L1
Woods T. E., Gilfanov M., 2016, MNRAS, 455, 1770
Woosley S. E., Kasen D., 2011, ApJ, 734, 38
Woosley S. E., Weaver T. A., 1994, ApJ, 423, 371
Yang Y. et al., 2018, ApJ, 852, 89
Yuan F., Kobayashi C., Schmidt B. P., Podsiadlowski P., Sim S. A., Scalzo R. A., 2013, MNRAS, 432, 1680

This paper has been typeset from a TEX/LATEX file prepared by the author.